JOURNAL OF MATERIALS SCIENCE 32 (1997) 1277–1285

Predicting Hertzian fracture

A. C. FISCHER-CRIPPS
Department of Applied Physics, University of Sydney, NSW 2006, Australia

The procedure for calculating the probability of initiation of a Hertzian cone crack as a function of indenter load and indenter radius is demonstrated and the results compared with experimental data. Such a procedure brings together the energy balance and flaw statistical explanations of Auerbach's law. The method relies on the application of Weibull statistics in the diminishing indentation stress field. It is shown how strength parameters obtained from bending tests on bulk specimens may be used within the analysis for predicting the presence of surface flaws which lead to the initiation of a cone crack. The procedure is shown to apply to both cylindrical punch and spherical indenters.

1. Introduction

Indentation fractures in glass were first studied in detail by Hertz [1, 2] in 1881. Hertz found that a cone crack of characteristic appearance occurred in a flat specimen of glass which was loaded by a hard, spherical indenter. In 1891, Auerbach [3] noted that a cone crack appears when the force reaches a critical value which is directly proportional to the radius of the indenter, a relationship often referred to as "Auerbach's law". Early analyses appeared to indicate that Auerbach's law contradicts the Griffith energy balance criterion for crack growth. Attempts to explain Auerbach's law in terms of the statistical spread of surface flaw sizes [4] were largely unsuccessful. In 1967, Frank and Lawn [5] proposed an energy balance analysis, independent of the surface flaw statistics, which was extensively revised in 1984 by Mouginot and Maugis [6]. In 1994, Fischer-Cripps and Collins [7] showed that the probability of initiation of a Hertzian cone crack in a specimen with a given surface flaw distribution could only be determined by a consideration of *both* the energy balance analysis and the surface flaw statistics. Fischer-Cripps and Collins gave particular attention to the case of cylindrical flat punch indenters using an indentation stress field obtained from a finite element analysis. The present work is concerned with a demonstration of the procedure given by these workers and its application to the case of both spherical and cylindrical flat punch indenters using analytically derived indentation stress fields.

2. The indentation stress field

Hertz observed that for spherical indenters, cone cracks always started near the edge of the contact circle where the tensile stresses were the greatest and formulated mathematical relationships between indenter load P, the indenter radius R, contact area a

$$a^3 = \frac{4}{3}\frac{kPR}{E} \tag{1a}$$

where k is an elastic mismatch constant

$$k = \frac{9}{16}\left[(1-\nu^2)+\frac{E}{E'}(1-\nu'^2)\right] \tag{1b}$$

In these equations, E and E' is Young's modulus, and ν and ν' is Poisson's ratio of the specimen and the indenter respectively. Fig. 1 shows the geometry of the contact for both spherical and cylindrical indenters.

Hertz did not calculate the magnitudes of the stresses at general points within the specimen but offered a suggestion as to their character by interpolating between those he calculated on the surface and along the axis of symmetry. The indentation stress field for the case of a spherical indenter appears to have been first calculated in detail by Huber [8] in 1904 and again later by Fuchs [9] in 1913, Huber and Fuchs [10], 1914, and Moreton and Close [11] in 1922. More recently, the integral transform method of Sneddon [12] has been applied to axis-symmetric distributions of normal pressures which correspond to a variety of indenters [13]. An extensive mathematical treatment is given by Gladwell [14], and an accessible text directed to practical applications is given by Johnson [15]. In the present work, we require the indentation stress field for spherical and cylindrical flat punch indenters and we refer directly to literature sources.

For the case of a spherical indenter, the distribution of stress within the specimen, in cylindrical coordinates, is given by [8, 16]

$$\frac{\sigma_r}{p_m} = \frac{3}{2}\left\{\frac{1-2\nu}{3}\frac{a^2}{r^2}\left[1-\left(\frac{z}{u^{1/2}}\right)^3\right]+\left(\frac{z}{u^{1/2}}\right)^3 \frac{a^2u}{u^2+a^2z^2}+\frac{z}{u^{1/2}}\left[u\frac{1-\nu}{a^2+u} + (1+\nu)\frac{u^{1/2}}{a}\tan^{-1}\left(\frac{a}{u^{1/2}}\right)-2\right]\right\} \tag{2a}$$

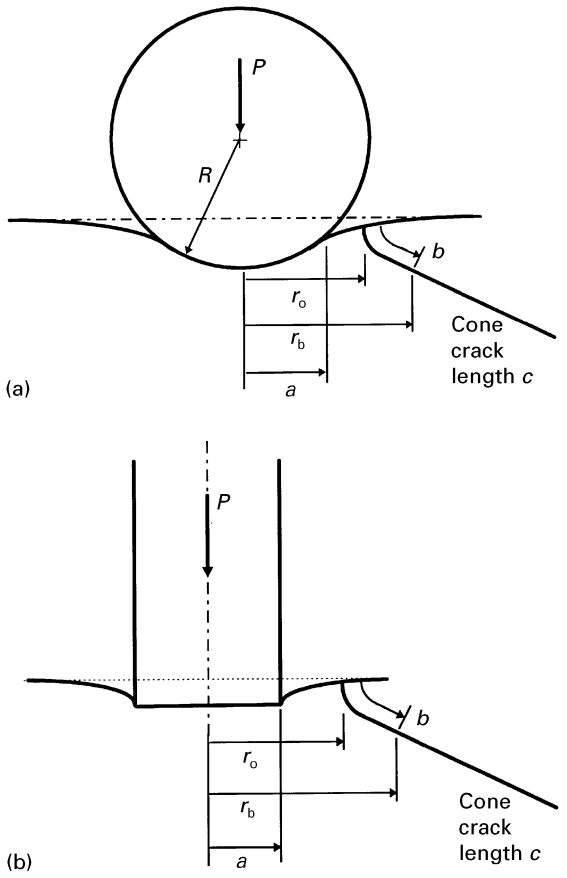

Figure 1 Geometry of indentation fracture with (a) spherical and (b) cylindrical flat punch indenters.

$$\frac{\sigma_\theta}{p_m} = -\frac{3}{2}\left\{\frac{1-2\nu}{3}\frac{a^2}{r^2}\left[1-\left(\frac{z}{u^{1/2}}\right)^3\right] + \frac{z}{u^{1/2}}\left[2\nu + u\frac{1-\nu}{a^2+u} - (1+\nu)\frac{u^{1/2}}{a}\tan^{-1}\left(\frac{a}{u^{1/2}}\right)\right]\right\} \quad (2b)$$

$$\frac{\sigma_z}{p_m} = -\frac{3}{2}\left(\frac{z}{u^{1/2}}\right)^3\left(\frac{a^2u}{u^2+a^2z^2}\right) \quad (2c)$$

$$\frac{\tau_{rz}}{p_m} = -\frac{3}{2}\left(\frac{rz^2}{u^2+a^2z^2}\right)\left(\frac{a^2u^{1/2}}{a^2+u}\right) \quad (2d)$$

where

$$u = \tfrac{1}{2}\{(r^2+z^2-a^2) + [(r^2+z^2-a^2)^2 + 4a^2z^2]^{1/2}\} \quad (2e)$$

In Equation 2, $p_m = P/\pi a^2$ is the mean contact pressure, with P equal to the indenter load, and a is the radius of the circle of contact. The principal stresses, in the rz plane are given by

$$\sigma_{1,3} = \frac{\sigma_r+\sigma_z}{2} \pm \left\{\left[\frac{(\sigma_r-\sigma_z)}{2}\right]^2 + \sigma_{rz}^2\right\}^{1/2}$$

$$\sigma_2 = \sigma_\theta$$

$$\tau_{max} = \tfrac{1}{2}(\sigma_1-\sigma_3) \quad (3a)$$

and the angle between the direction of σ_1 and the surface of the specimen is found from

$$\frac{dz}{dr} = -\frac{\sigma_r-\sigma_z}{2\tau_{rz}} \pm \left[\left(\frac{\sigma_r-\sigma_z}{2\tau_{rz}}\right)^2 + 1\right]^{1/2} \quad (3b)$$

where $\pm$ is the sign of τ_{rz} [13].

On the surface (at $z = 0$ and all values of r/a), and also beneath the indenter along the z axis at $r = 0$, σ_r, σ_θ, σ_z are principal stresses. The hoop stress, σ_θ, is always a principal stress because of symmetry. On the surface of the specimen, beneath the indenter ($r < a$), all three principal stresses are compressive and all have approximately the same magnitude. Outside the contact circle but still on the surface, the first principal stress $\sigma_1 = \sigma_r$ is tensile with a maximum value at the edge of the contact circle. This stress is usually responsible for the formation of Hertzian cone cracks. The second principal stress, $\sigma_2 = \sigma_\theta$ is a hoop stress and is compressive in this region. Outside the contact area along the surface, $\sigma_2 = -\sigma_1$ and beneath the surface along the axis of symmetry at $r = 0$, the two principal stresses are equal, $\sigma_2 = \sigma_1$. The magnitude of σ_3 at the surface is zero outside the contact circle since it acts normal to a free surface in this region. Along the surface, at all values of r/a, $\sigma_1 = \sigma_r$ and acts in a radial direction. σ_2 is of course a hoop stress, and σ_3 acts normal to the surface. It is convenient to label the stresses such that $\sigma_1 > \sigma_2 > \sigma_3$ nearly always.

Fig. 2a–c shows contours of equal values of stress calculated using the Equations 2 and 3. Note that the contours shown in Fig. 2a–c give no information about the direction or line of action of these stresses. Such information is only available by examining stress trajectories. Stress trajectories are curves whose tangents show the direction of one of the principal stresses at the point of tangency and are particularly useful in visualizing the directions in which the principal stresses act. The stress trajectories of σ_2, being a hoop stress, are circles around the z axis. Stress trajectories for σ_1 and σ_3 can be determined from Equation 3b and are shown in Fig. 2d.

The important feature of the indentation stress field for the initiation of a conical fracture in brittle materials is the tensile region in the specimen surface just outside the area of contact. Hertzian cone cracks tend to follow a direction of orthogonality with the greatest value of tensile stress, i.e. σ_1. Thus, it is not surprising to observe that cone cracks, as they travel downward into the specimen, appear to follow the σ_3 stress trajectory which itself is orthogonal to the σ_1 trajectory. As demonstrated by Frank and Lawn [5], it is this feature of the geometry of the cone cracks that allows us to determine the strain energy release rate along the path of the σ_3 stress trajectory.

As for the case of a sphere, the stress distribution within the specimen loaded by a cylindrical punch is given in cylindrical coordinates, with stresses expressed in terms of the mean contact pressure and spatial coordinates normalized to the contact radius a, as follows

$$\frac{\sigma_r}{p_m} = -\frac{1}{2}\left[J_1^0 - \frac{z}{a}J_2^0 - (1-2\nu)\frac{a}{r}J_0^1 + \frac{z}{r}J_1^1\right] \quad (4a)$$

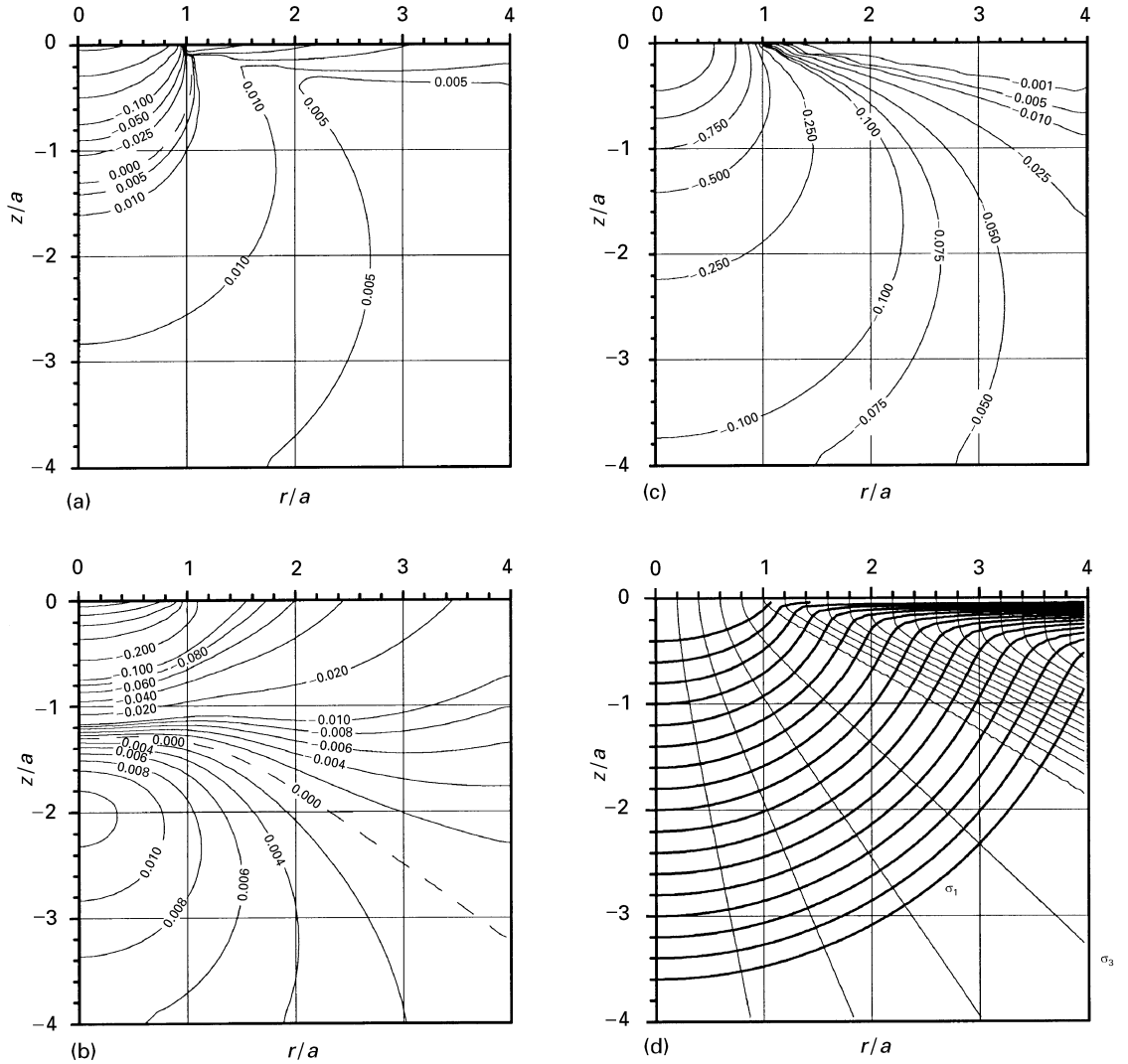

Figure 2 Stress trajectories and contours of equal stress for spherical indenter calculated for Poisson's ratio $\nu = 0.26$. Distances r and z normalized to the contact radius a and stresses expressed in terms of the mean contact pressure p_m. (a) σ_1, (b) σ_2, (c) σ_3, (d) σ_1 and σ_3 trajectories.

$$\frac{\sigma_\theta}{p_m} = -\frac{1}{2}\left[2\nu J_1^0 + (1-2\nu)\frac{a}{r}J_0^1 - \frac{z}{r}J_1^1\right] \quad (4b)$$

$$\frac{\sigma_z}{p_m} = -\frac{1}{2}\left[J_1^0 + \frac{z}{a}J_2^0\right] \quad (4c)$$

$$\frac{\tau_{rz}}{p_m} = -\frac{1}{2}\frac{z}{a}J_2^1 \quad (4d)$$

where

$$J_1^0 = R^{-1/2}\sin\frac{\phi}{2}$$

$$J_0^1 = \frac{a}{r}\left(1 - R^{1/2}\sin\frac{\phi}{2}\right)$$

$$J_2^1 = \frac{r}{a}R^{-3/2}\sin\frac{3\phi}{2}$$

$$J_2^0 = \left(1+\frac{z^2}{a^2}\right)^{1/2}R^{3/2}\sin\left(\frac{3\phi}{2}-\theta\right)$$

$$J_1^1 = \left(1+\frac{z^2}{a^2}\right)^{1/2}\frac{a}{r}R^{-1/2}\sin\left(\theta-\frac{\phi}{2}\right)$$

$$R = \left[\left(\frac{r^2}{a^2}+\frac{z^2}{a^2}-1\right)^2 + 4\frac{z^2}{a^2}\right]^{1/2}$$

$$\tan\phi = 2\frac{z}{a}\left(\frac{r^2}{a^2}+\frac{z^2}{a^2}-1\right)^{-1}$$

$$\tan\theta = \frac{a}{z} \quad (4e)$$

Note that the factor R in Equation 4e is equivalent to u in Equation 2e. Principal stresses and maximum shear stresses can be found by substituting Equations 4a to 4d into Equation 3a, where appropriate. Stress contours and trajectories for the case of a cylindrical punch indenter are shown in Fig. 3.

3. Fracture mechanics in the indentation stress field

The well-known Griffith [17] criterion for fracture relates the energy needed to form new crack surfaces and the attendant release in strain energy. The externally applied uniform stress σ_a required for the growth of an existing flaw of length $2c$ and unit width is

$$\sigma_a \geqslant \left[\frac{2\gamma E}{(1-\nu^2)\pi c}\right]^{1/2} \quad (5)$$

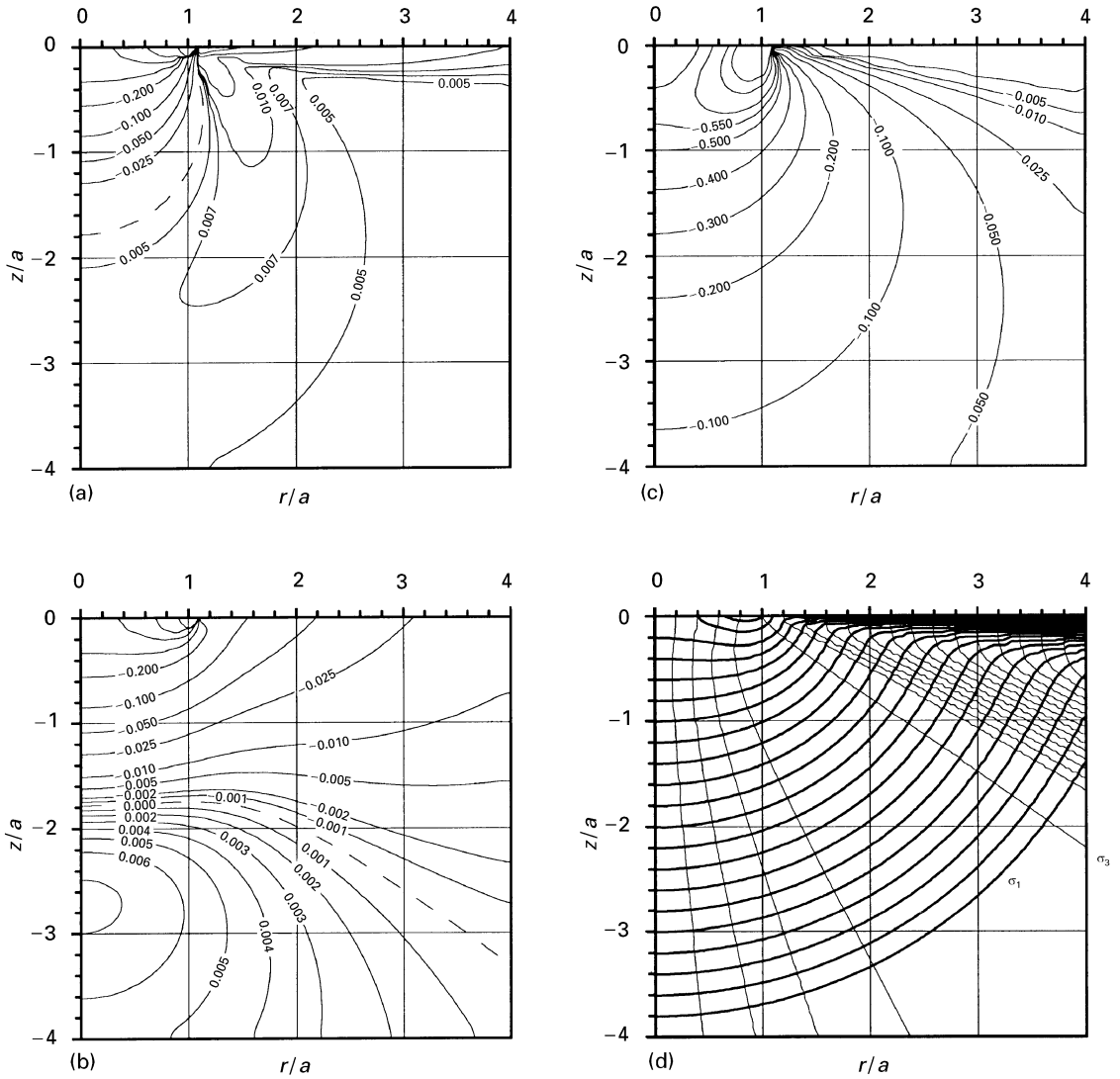

Figure 3 Stress trajectories and contours of equal stress for cylindrical flat punch indenter calculated for Poisson's ratio $\nu = 0.26$. Distances r and z normalized to the contact radius a and stresses expressed in terms of the mean contact pressure p_m. (a) σ_1, (b) σ_2, (c) σ_3, (d) σ_1 and σ_3 trajectories.

where γ is the *fracture* surface energy in $J\,m^{-2}$. The $1 - \nu^2$ term is included for the general case of plane strain. Equation 5 applies directly to a double-ended crack of length $2c$ contained fully within a uniformly stressed solid where the stress is applied normal to the crack. It may also be applied with only a small error to a half crack of length c, such as may be found on the surface of a solid.

The Griffith criterion is more commonly stated in terms of Irwin's stress intensity factor [18] K_1 where

$$\frac{K_1^2(1-\nu^2)}{E} \geqslant 2\gamma \tag{6}$$

where, for the case of an infinite solid

$$K_1 = \sigma(\pi c)^{1/2} \tag{7}$$

The left-hand side of Equation 6 is termed the strain energy release rate and is given the symbol G. The Griffith criterion is satisfied for $K_1 \geqslant K_{1C}$ where K_{1C} may be considered a material property which can be readily measured in the laboratory. A typical value for soda-lime glass is $0.78\ MPa\,m^{1/2}$. Using this value, Equations 6 and 7 give a fracture surface energy for soda-lime glass of $\gamma = 3.6\ J\,m^{-2}$, which is in agreement with various experimentally determined values of this quantity [19].

For the case of a crack in a non-uniform stress field, Frank and Lawn [5] showed that the stress intensity factor may be calculated using the prior stress field along the proposed crack path using

$$K_1 = \frac{2}{\pi^{1/2}} \int_0^c c^{1/2} \frac{\sigma(b)}{(c^2 - b^2)^{1/2}}\, db \tag{8}$$

where c is the length of the crack and b is the length of travel along the crack path. Frank and Lawn determined the stress intensity factor for a crack path which started at the radius of the circle of contact and followed the σ_3 stress trajectory down into the interior of the specimen. Mouginot and Maugis [6] applied Equation 8 for potential crack paths for a range of starting radii in the vicinity of the indenter. Their work showed that Auerbach's law is a consequence of the peculiar nature of the diminishing stress field which, together with the radius of the indenter, influences the starting radius of the cone crack and hence its subsequent progress through the bulk of the

specimen. They argued that for a high density of flaws of uniform size, the cone crack is initiated at the radius for which the strain energy release rate is greatest.

Equation 8 may be re-written with stresses in terms of the mean contact pressure p_m and distances expressed with respect to the contact radius a such that

$$f(b/a) = \frac{\sigma(b/a)}{p_m} \tag{9}$$

Combining Equations 8 and 9 and including a factor r_b/r_c which accounts for the expanding crack front we may define a function $\phi(c/a)$, related to K_{1C}, as

$$\phi(c/a) = \frac{c}{a}\left[\int_0^{c/a} \frac{r_b}{r_c}\left(\frac{c^2}{a^2} - \frac{b^2}{a^2}\right)^{-1/2} f(b/a)\,\mathrm{d}(b/a)\right]^2 \tag{10}$$

where $2\pi r_c$ represents the length of the crack front at the tip of the cone crack, and $2\pi r_b$ is the crack length at the point defined by the variable b at which $\sigma(b)$ applies.

Since $p_m = P/\pi a^2$, Equation 10, together with Equation 1, allows the Griffith criterion at the critical fracture condition for the case of the sphere to be expressed as

$$G = 2\gamma = \frac{3(1-\nu^2)P}{\pi^3 kR}\phi(c/a) \tag{11a}$$

and for either the sphere or punch in terms of a

$$G = 2\gamma = \frac{4(1-\nu^2)P^2}{\pi^3 Ea^3}\phi(c/a) \tag{11b}$$

The function $\phi(c/a)$ contains an integral which is characteristic of the pre-existing stress field. The function $\phi(c/a)$ must be evaluated for a particular starting radius, r_0/a, since this determines the values of the stress along the crack path.

Rearranging Equation 11b gives the critical load for fracture, for either the sphere or the punch

$$P_c = \left(\frac{a^3}{\phi(c/a)}\right)^{1/2}\left(\frac{\pi^3 E 2\gamma}{4(1-\nu^2)}\right)^{1/2} \tag{12}$$

where it is noted that the factors in the second term on the far right-hand side of Equation 12 are all material constants. For both the sphere and the punch, there is a range of values of stress level, indenter radius and flaw sizes for which $\phi(c/a)$ is nearly constant and leads to Auerbach's law.

Fig. 4 shows values for σ_1 along the path of the σ_3 stress trajectory for different starting radii for both spherical and flat punch indenters and demonstrates the diminishing stress field along the prospective crack paths. The integral in Equation 10 may be evaluated numerically for the stress distribution along each σ_3 stress trajectory and plotted as a function of c/a as shown in Fig. 5. The value of $\phi(c/a)$ for any particular normalized radius r_0/a is proportional to the strain energy release rate for a crack of size c/a which commences at that radius r_0/a. For any flaw size c_f, there is a particular radius, r_0, for which the strain energy release rate is greatest. This corresponds to the upper envelope of the curves of $\phi(c/a)$ in Fig. 5. This upper

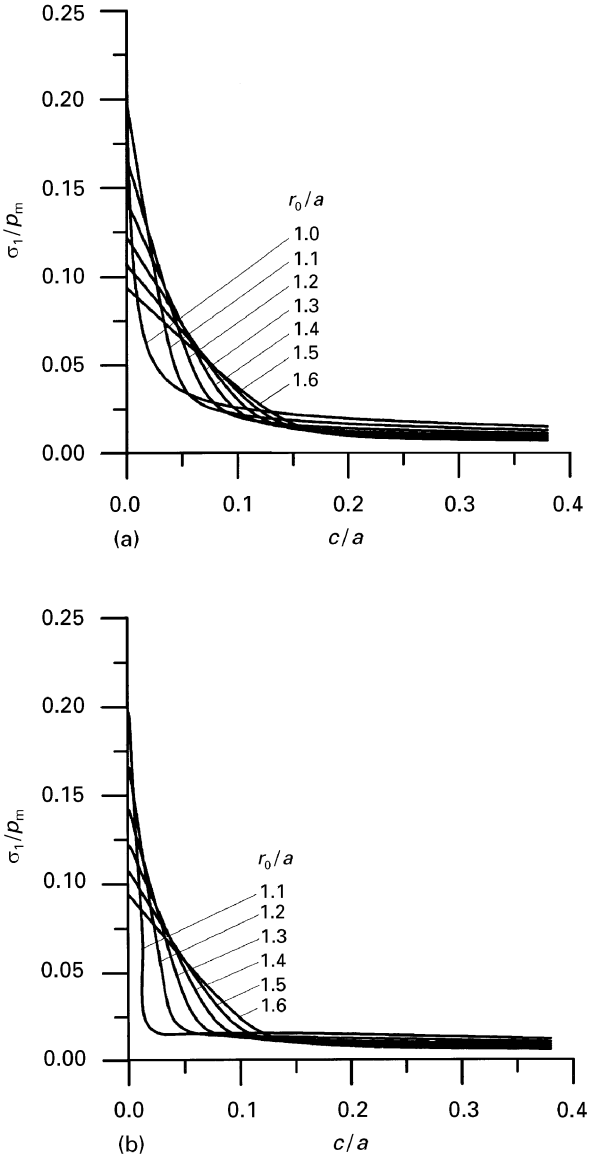

Figure 4 Normalized radial stress σ_1/P_m plotted as a function of normalized distance c/a along the σ_3 stress trajectory for different starting radii, r_0/a for (a) spherical indenter and (b) cylindrical flat punch indenter. Stresses and trajectories calculated for $\nu = 0.26$.

envelope, not drawn in these figures, is denoted as $\phi(c_f/a)$. When the indenter load is steadily increased, the Griffith criterion will be first met when the strain energy release rate, given by Equations 11a and 11b with the envelope of the curves, $\phi(c_f/a)$, becomes equal to twice the fracture surface energy. A cone crack will initiate at the lowest load for which a flaw of size c_f/a exists in the specimen at a radius for which $\phi(c_f/a)$ is greater than the critical value.

For flaws within the Auerbach range of flaw sizes, the minimum critical load is given the symbol P_a and is found from

$$P_a = \left[\frac{k2\gamma\pi^3}{3(1-\nu^2)\phi_a}\right]R \tag{13a}$$

for the sphere and

$$P_a = \left[\frac{E\pi^3\gamma}{(1-\nu^2)2\phi_a}\right]^{1/2} a^{3/2} \tag{13b}$$

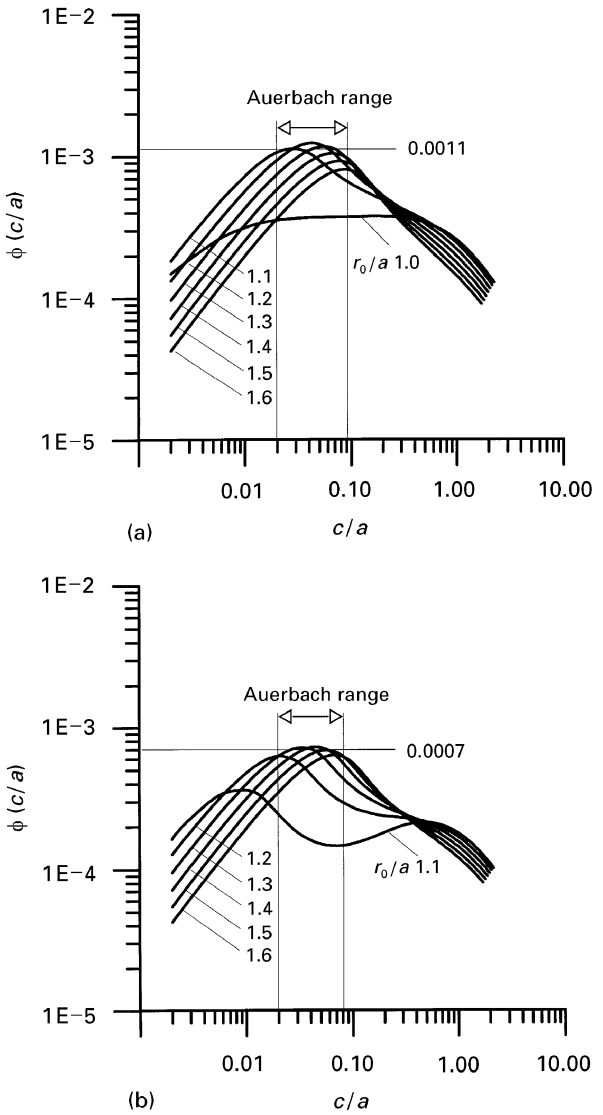

Figure 5 Strain energy release function $\phi(c/a)$ as a function of normalized crack length, c/a, for different starting radii, r_0/a for (a) spherical indenter and (b) cylindrical flat punch indenter. The Auerbach range where the outer envelope of $\phi(c/a)$ is approximately constant, is indicated in each figure along with the estimated value of ϕ_a.

for the punch where the term in the square brackets in Equation 13a, is the Auerbach constant. In Equations 13a and 13b, ϕ_a is the value of $\phi(c/a)$ at the plateau. From Fig. 5, this is estimated to be at $\phi(c/a) = 0.0011$ for the case of the sphere and $\phi(c/a) = 0.0007$ for the punch. The value of ϕ_a is important since it influences the fracture surface energy which is estimated from data obtained from experiments. Combining Equations 11 and 13, it may be shown that

$$\frac{G}{2\gamma} = \left(\frac{P}{P_a}\right)\frac{\phi(c/a)}{\phi_a} \tag{14a}$$

for the sphere and

$$\frac{G}{2\gamma} = \left(\frac{P}{P_a}\right)^2\frac{\phi(c/a)}{\phi_a} \tag{14b}$$

for the case of the punch.

The term "fracture" in the present context signifies the extension of a flaw to a circular ring crack concentric with the contact radius. Once a flaw has become a propagating crack, it extends according to the strain energy release function curve (Fig. 5) appropriate to its starting radius. The development of this starting flaw into a ring crack precludes the extension of other flaws in the vicinity, even though the value of $\phi(c/a)$ for those flaws at some applied load above the flaw initiation load may be larger than that calculated for the starting flaw as it follows its $\phi(c/a)$ curve. This is because the conditions which determine crack growth depend on the *prior* stress field. The function $\phi(c/a)$ can be used to describe the initiation of crack growth for all flaws which exist in the prior stress field but can only be considered applicable for the subsequent elongation for that flaw which actually first extends.

4. Calculating the probability of Hertzian fracture

Both the size and distribution of surface flaws characterize the strength of brittle solids and the probability of failure of a specimen of surface area A subjected to a uniform tensile stress σ can be calculated using Weibull statistics [20]

$$P_f = 1 - \exp(-kA\sigma^m) \tag{15}$$

where m and k are the Weibull parameters. The parameter m describes the spread in strengths (a large value indicating a narrow range) and the parameter k is associated with the "reference strength" and the surface flaw density of the specimen. In the present work, we use $m = 7.3$ and $k = 5.1 \times 10^{-57}\ \mathrm{m}^{-2}\,\mathrm{Pa}^{-7.3}$ as determined by Brown [21] for as-received soda-lime glass.

The probability of failure given by Equation 15 is equal to the probability of finding a flaw within an area A of the specimen surface which is larger than the critical flaw size (as given by the Griffith criterion) for a uniform stress σ. The critical flaw size is given by Equation 7 with $K_1 = K_{1C}$.

We are now in a position to calculate the probability of fracture for a given load and radius of indenter. Let P_a be the minimum critical load for values of c/a within the Auerbach range. As noted above, the value of ϕ_a corresponding to P_a can be estimated by inspection of Fig. 5. The normalized strain energy release rate $G/2\gamma$ may be determined from Equations 11a and 11b or Equations 14a and 14b. The Griffith criterion is met when $G/2\gamma \geqslant 1$. If the load P is less than the minimum critical load P_a, failure will not occur from any flaws, no matter how large, since the Griffith criterion is never met. Fracture from flaws of size below, including, and beyond the Auerbach range can only occur if the load is greater than P_a.

At a load P greater than P_a, the Griffith criterion is met for various ranges of flaw sizes which depend on the particular values of starting radii. Fracture will occur from a flaw located at a particular starting radius if that flaw is within the range for which $G/2\gamma \geqslant 1$ for that radius. This range of flaw sizes can be determined fom Fig. 5 and is given by the c/a axis coordinates for the upper and lower bounds of the region where $\phi(c/a)$ is such that $G/2\gamma > 1$ for the curve which corresponds to the radius r_0 under

consideration. The problem has been reduced to that from calculating the probability of indentation fracture occurring at a particular radius and load to the probability of finding at least one flaw within a specific size range at that radius. For the case of a punch, the procedure is straight forward since the radius of circle of contact, a, is a constant. For a sphere, the contact radius depends upon the load and the procedure for determining the required flaw sizes is slightly more complicated.

To determine these probabilities, it is convenient to divide the area surrounding the indenter into n annular regions of radii r_i ($i = 1$ to n). To determine the probability of finding a flaw which meets the Griffith criterion within each annular region, Equation 15 may be used. Equation 15 gives the probability of failure for an applied uniform stress, but also can be used to calculate the probability of finding a flaw of size greater than or equal to the critical value for that stress, as given by Equation 7, within an area A of the surface of the solid. The strength parameters, m and k, for Equation 15 are those which are appropriate to the specimen surface condition. The probabilities calculated for each annular region can be suitably combined to yield a total probability of failure for a particular indenter load and radius for a given surface flaw distribution.

Let us first consider the case of a flat punch of radius a. Consider an annular region of the specimen surface with radius r_i and area δA_i. The load applied to the indenter is set to some desired value of P/P_a. The range of values of flaw size which satisfies the Griffith criterion may be determined for this region by considering the appropriate line for $\phi(c/a)$ in Fig. 5. That is, $G/2\gamma$ is calculated for a range of c/a using Equation 14b and the range of c/a, and hence c_f, for which $G/2\gamma \geqslant 1$ is identified. Let the range of flaw sizes of interest be denoted by $c_1 \leqslant c \leqslant c_2$. We therefore require the probability of finding such a flaw within this size range in the area δA. This is equal to the difference between the probability of finding a flaw of size $c > c_1$ and the probability of finding a flaw of size $c > c_2$. However, the probability of finding a flaw of size greater than a specific size, say c_1, within the area δA_i is equal to the Weibull probability of failure under the corresponding critical stress as given by Equation 7.

For a given radius of indenter, the probability of finding a flaw of size greater than c_1 within the annular region of radius r_i and width δr_i, which has an area $\delta A_i = 2\pi r_i \delta r_i$, is

$$P_i(c > c_1) = 1 - \exp\left\{ - k2\pi r_i \delta r_i \left[\frac{K_{1C}}{(\pi c_1)^{1/2}} \right]^m \right\} \quad (16)$$

with a similar expression for $P_i(c > c_2)$. The probability of finding a flaw of size in the range $c_1 \leqslant c \leqslant c_2$ within area δA_i is the difference in probabilities and is equal to the probability of failure from a flaw of size within that range

$$P_{f_i}(c_1 \leqslant c \leqslant c_2) = P_i(c > c_1) - P_i(c > c_2) \quad (17)$$

The values c_1 and c_2 may be determined for all annular regions, i.e. values of r_0/a, by repeating the above procedure. The probability of fracture not occurring from a flaw within the region δA is found from

$$P_{s_i} = 1 - P_{f_i} \quad (18)$$

The probability of survival for the entire region of n annular elements surrounding the indenter is thus given by

$$P_S = P_{s_1} P_{s_2} P_{s_3} \ldots P_{s_i} \ldots P_{s_n} \quad (19)$$

Therefore finally, the probability of failure P_F for the entire region, at the load P/P_a, is then given by

$$P_F = 1 - P_S \quad (20)$$

This calculation may be repeated for different values of P/P_a to obtain the probability of failure as a function of indenter load for a particular value of indenter radius.

For the case of a sphere, the situation is complicated by the expanding radius of circle of contact with increasing load. Combining Equations 1 and 13a, it is easy to show that the radius of circle of contact for a given radius of indenter and ratio P/P_a may be calculated from

$$a^3 = \frac{8}{9}\frac{k^2}{E}\frac{\gamma\pi^3}{(1-\nu^2)\phi_a}\frac{P}{P_a}R^2 \quad (21)$$

thus permitting values for c_f to be determined as a function of P/P_a for a constant R and proceeding as for the case of the punch.

Fig. 6 shows the probability of failure as a function of indenter load for a particular size of indenter for both spherical and cylindrical punch indenters for as-received glass. Calculated values are shown along with those determined from indentation experiments [7]. Agreement is fairly good especially when one considers that the Weibull parameters used in the calculations were determined on glass specimens from a completely different source to those used in the experimental work presented here. The curves in Fig. 6 rely on an estimation of the fracture surface energy γ in Equations 13a and 13b. Although the fracture surface energy may in principle be determined from indentation tests, such estimations are inaccurate due to the inevitable presence of friction between the indenter and the specimen. Fischer-Cripps and Collins [7] included an adjustment factor $\beta = 2.5$ in their analysis to account in a simple manner for the effect of friction. The calculated curves in Fig. 6 have been obtained from Equations 13a and 13b with fracture surface energies determined from the experimental data (see below) which correspond to $\beta \approx 2$.

5. Fracture surface energy and the Auerbach constant

The procedure given in previous sections for calculating the probability of initiation of a Hertzian cone crack relies upon an estimation of the fracture surface energy of the specimen material. Experimental work reported by Fischer-Cripps and Collins [7] indicates

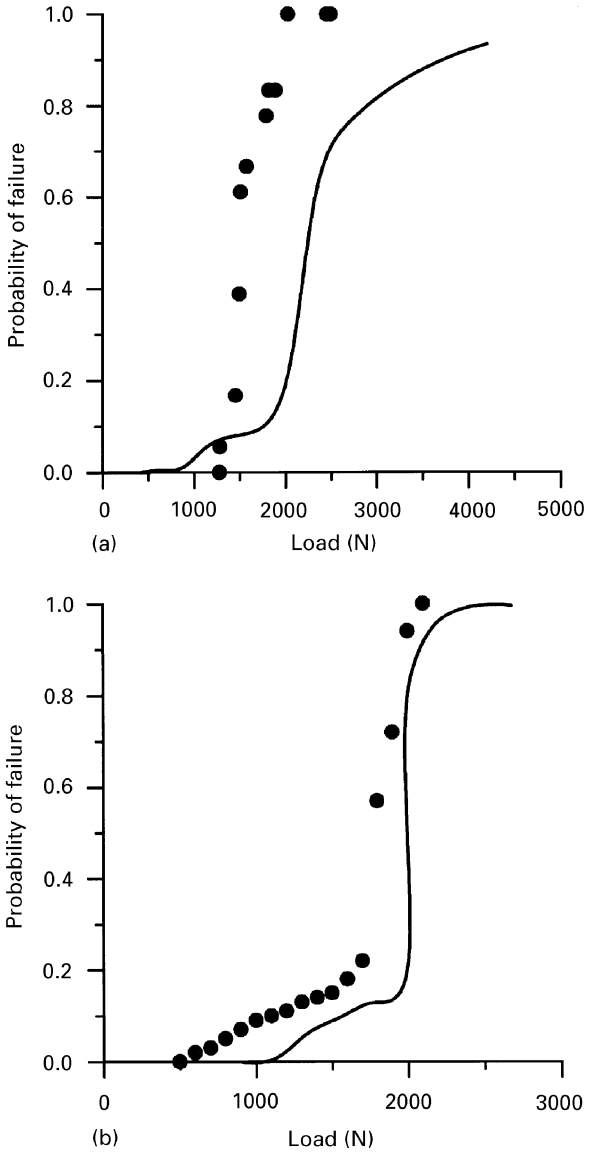

Figure 6 Probablity of failure versus indenter load for as-received soda-lime glass for (a) spherical indenter $R = 4$ mm and (b) cylindrical flat punch indenter $a = 0.4$ mm. Solid line indicates calculated values with surface energy γ as given in Table I and (●) indicates experimental results with lubricated contacts.

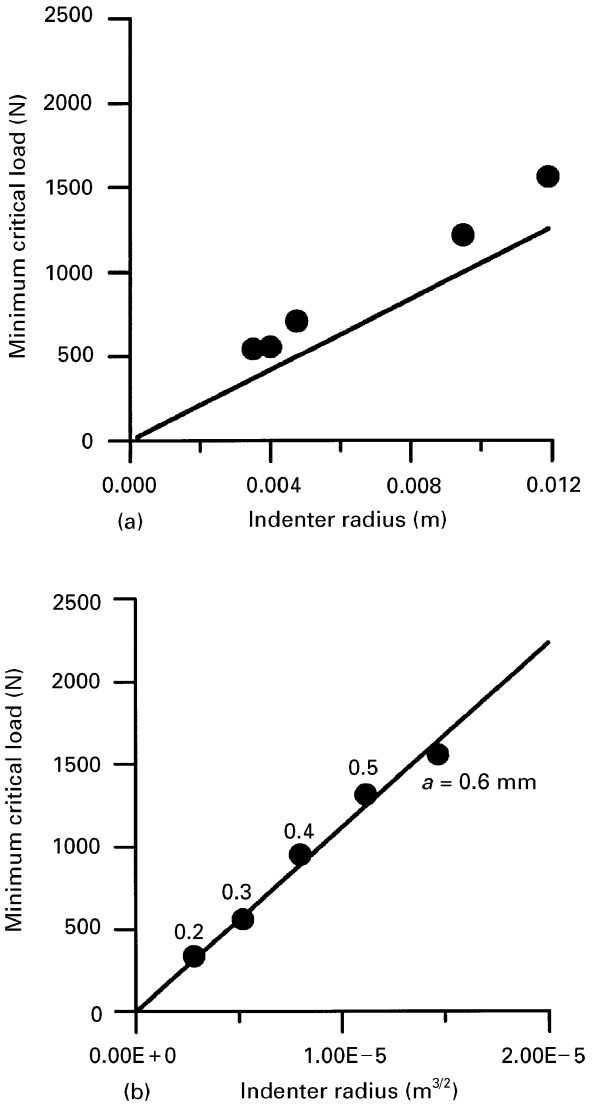

Figure 7 Minimum critical load versus indenter radius for (a) spherical and (b) cylindrical indenters for abraded soda-lime glass with lubricated contacts. The horizontal axis in (b) is given as the indenter radius raised to the 2/3 power. Solid line indicates calculated values with surface energy γ as given in Table I and (●) indicates experimental results. In (b), the actual radius of the indenter in mm is shown for each experimental result.

a fracture surface energy nearly 2.5 times that determined by other means [19], causing those workers to postulate that the inevitable presence of friction beneath the indenter leads to an increase in the apparent surface energy estimated from indentation experiments, even with lubricated contacts. Estimations of fracture surface energy are best undertaken with respect to the minimum critical load for failure.

As before, let P_a denote the minimum critical load for an indentation fracture to occur. We would expect this minimum critical load to correspond to the fracture load observed in experiments on glass with a high density of flaws, i.e. on abraded glass. Equations 13a and 13b predict a straight line relationship between spherical indenter radius and the punch radius to the 3/2 power respectively and the minimum critical load. This is expected since Equations 13a and 13b assume a specimen surface containing flaws of all sizes and do not give any information about the probability of finding a particular sized flaw at a particular starting radius. As the indenter size is increased, the flaw size corresponding to the Auerbach range also increases and it is from flaws within the Auerbach range that failure first occurs – since the function $\phi(c/a)$, as shown in Fig. 5a and b, are a maximum in the Auerbach range of flaw sizes.

From Equation 13a, the Auerbach constant is given by

$$A = \left[\frac{k2\gamma\pi^3}{3(1-\nu^2)\phi_a}\right] \tag{22a}$$

For the case of the punch, the Auerbach constant for a sphere of radius R giving a contact circle of radius a may be found from Equation 13b

$$A = \left[\frac{E\pi^3\gamma}{(1-\nu^2)2\phi_a}\right]\left(\frac{4k}{3E}\right) = \frac{2k\pi^3\gamma}{(1-\nu^2)\phi_a} \tag{22b}$$

TABLE I Calculated fracture surface energy and Auerbach constant for soda-lime glass from indentation tests with spherical and cylindrical flat punch indenters

	Sphere	Punch
Fracture surface energy ($J\,m^{-2}$)	8.88	7.46
Auerbach constant ($N\,m^{-1}$)	105 233	138 848

As can be seen from Equations 22a and 22b, the Auerbach constant depends upon the value of fracture surface energy γ. Fig. 7 shows experimental data for the minimum critical load obtained on abraded soda-lime glass using both spherical and flat punch indenters. The data for the punch has been plotted as a function of $a^{3/2}$ so as to give a linear relationship with the minimum critical load, and the actual punch diameter is indicated for each data point. The slope of line of best fit through this data is then directly proportional to the fracture surface energy. Values of γ estimated in this manner are given in Table I together with the calculated Auerbach constants for each type of indenter.

As can be seen, the fracture surface energies obtained using this method for the two indenters are not all that much different although they are appreciably higher than the expected value of $\gamma = 3.5\,J\,m^{-2}$ for this material. The difference, as postulated by Fischer-Cripps and Collins [7], is probably due to friction between the indenter and the specimen during testing. Differences between the value obtained from the experiments using the sphere and that with the punch are due to the different dependence on friction on the indentation response of the two types of indenter. The solid lines in Fig. 7a and b have been calculated using Equations 13a and 13b with the fracture surface energies as shown in Table I for each type of indenter.

Although the theory predicts that, within the Auerbach range there is a linear relationship between the minimum critical load and the indenter radius, there is no particular reason why this should be so for median or mean fracture loads. Indeed, if a linear relationship were to exist, it would be expected that the Auerbach constants obtained from such data would be largely determined by the flaw statistics of the sample, rather than by intrinsic material properties.

6. Conclusions

The procedure for calculating the probability of initiation of a Hertzian cone crack as a function of indenter load and indenter radius has been demonstrated and the results compared with experimental data. Such a procedure brings together the energy balance and flaw statistical explanations of Auerbach's law. The method relies on the application of Weibull statistics in the diminishing indentation stress field. Strength parameters obtained from bending tests on bulk specimens may be used within the analysis for predicting the presence of surface flaws which lead to the initiation of a cone crack. The procedure given in the present work has been shown to apply to both cylindrical punch and spherical indenters.

Acknowledgements

The author wishes to acknowledge Professor R. E. Collins of the University of Sydney for stimulating the work reported in this paper. This work was supported in part by His Royal Highness Prince Nawaf bin Abdul Aziz of the Kingdom of Saudi Arabia through the Science Foundation for Physics at the University of Sydney, and by the Australian Energy Research and Development Corporation.

References

1. H. HERTZ, *J. Reine Angew. Math.* **92** (1881) 156; Translated and reprinted in English in "Hertz's Miscellaneous Papers" (Macmillan & Co, New York, 1896) Ch. 5.
2. H. HERTZ, *Verhandlungen des Vereins zur Beforderung des Gewerbe Fleisses* **61** (1882) 449; Translated and reprinted in English in "Hertz's Miscellaneous Papers" (Macmillan & Co, New York, 1896) Ch. 6.
3. F. AUERBACH, *Annalen de Physik* (*Leipzig*) **43** (1891) 61.
4. B. HAMILTON and R. RAWSON, *J. Mech. Phys. Solids* **18** (1970) 127.
5. F. C. FRANK and B. R. LAWN, *Proc. Roy. Soc.* **A229** (1967) 291.
6. R. MOUGINOT and D. MAUGIS, *J. Mater. Sci.* **20** (1985) 4354.
7. A. C. FISCHER-CRIPPS and R. E. COLLINS, *ibid.* **29** (1994) 2216.
8. M. T. HUBER, *Ann. d. Phys.* **43** (1904) 61.
9. S. FUCHS, *Physik Zeitschr* **14** (1913) 1282.
10. M. T. HUBER and S. FUCHS, *ibid.* **15** (1914) 298.
11. W. B. MORETON and L. J. CLOSE, *Phil. Mag.* **43** (1922) 320.
12. I. N. SNEDDON, "Fourier transforms" (McGraw-Hill, New York, 1951).
13. M. BARQUINS and D. MAUGIS, *Journal de Mecanique theorique et appliquee* **1** (1982) 331.
14. G. M. L. GLADWELL, "Contact problems in the classical theory of elasticity" (Sijthoff and Noordhoff, Leyden, The Netherlands, 1980).
15. K. L. JOHNSON, "Contact mechanics" (Cambridge University Press, Cambridge, 1985).
16. B. R. LAWN, T. R. WILSHAW and N. E. W. HARTLEY, *Int. J. Fract.* **10** (1974) 1.
17. A. A. GRIFFITH, *Phil. Trans. Roy. Soc.* **A221** (1920) 163.
18. G. R. IRWIN, in "Handbuch der physik" **6** (Springer-Verlag, Berlin, 1958) p. 551.
19. S. W. FREIMAN, T. L. BAKER and J. B. WACHTMAN, Jr, in "Strength of inorganic glass" edited by C. R. Kurkjian (Plenum Press, New York, 1985) p. 597.
20. W. WEIBULL, "A statistical theory of the strength of materials", Handlingar Nr 151 (Ingeniors Vetenskaps Akademins, Stockholm, 1939).
21. W. G. BROWN, "A load duration theory for glass design", Publication No. NRCC 12354 (National Research Council of Canada, Division of Building Research, Ottawa, Canada, 1972).

Received 18 August 1995
and accepted 31 July 1996